Production of Cluster Complexes by Cluster-Cluster Collisions
— Incorporation of a Size-Selected Cobalt Dimer Ion into a Neutral Argon Cluster

SCHOLARONE™
Manuscripts

Production of Cluster Complexes by Cluster-Cluster Collisions — Incorporation of a Size-Selected Cobalt Dimer Ion into a Neutral Argon Cluster

Hideho Odaka[1] and Masahiko Ichihashi[2,*]

1) East Tokyo Laboratory, Genesis Research Institute, Inc., 717-86 Futamata, Ichikawa, Chiba 272-0001, Japan
2) Cluster Research Laboratory, Toyota Technological Institute: in East Tokyo Laboratory, Genesis Research Institute, Inc., 717-86 Futamata, Ichikawa, Chiba 272-0001, Japan

*Corresponding Author
E-mail: ichihashi@clusterlab.jp

ABSTRACT

Cluster-cluster collision is one of the methods to produce multi-element cluster complexes, in which the mechanism of coalescence is not clear. We have built up an apparatus to study the low-energy collisions between a size-selected metal cluster ion and a neutral molecular cluster by using a merging-beam technique in a pulsed mode. By use of this apparatus, we demonstrate the production of the cluster complexes in the collision of a cobalt dimer ion with a neutral argon cluster as an example. In this collision, the cluster complexes, $Co_2^+Ar_n$ (n = 1–30), are observed and the size distribution is dependent on the relative velocity. The production efficiency of the cluster complexes is shown as a function of the relative velocity of the collision, and the incorporation process is explained on the basis of the electrostatic interaction and the hard-sphere interaction below and above the relative velocity of 200 m/s respectively.

1. Introduction

Multi-element clusters attract much interest because of their chemical and physical properties [1], and it is expected that they are utilized in the field of catalysis [2], optoelectronics [3], biomedicine [4], and so on. Actually their properties are critically dependent on the size, composition and atomic ordering, and it should be important to control the above parameters in order to enhance their functionality.

The synthesis of multi-element clusters involves complicated processes, and hence there is a variety of techniques available for producing different types of multi-element clusters. Typically, they are produced in the gas phase [5-7], in the colloidal solutions [8-10], and on the surfaces [11, 12]. In the past decade or so, the sequential pick-up of various atoms by helium droplets has been established as an important method [13-17]. This is not only applied to the formation of multi-element clusters in the droplets, but also applied to a non-destructive deposition of the clusters on solid surfaces. Then the size, composition and atomic ordering of the multi-element clusters produced depend on the production method significantly. One of the attractive ways to produce these multi-element clusters is to make use of low-energy collisions between clusters which consist of different elements under controlled conditions in the gas phase. Recently, Singh *et al.* have produced the cluster complexes composed of non-size-selected clusters (silicon clusters and silver clusters), which were generated separately by using magnetron sputter sources [18].

Physical aspects of the cluster complex formation have been studied in the gas phase by analogy with the nuclear fusion since 1990s [19-21]. Schmidt *et al.* have investigated the collision between sodium clusters by using a quantum mechanical−molecular dynamics method, and have revealed that the collision dynamics changes from the fusion to the deep inelastic collision according to the collision energy and the impact parameter. Campbell and co-workers have measured experimentally the fusion cross sections between C_{60}^{+} and C_{60} in the energy region of 60−300 eV, and have found that the cross section shows a maximum of ~2 Å^2 at the collision energy of 140 eV.

Recently we have built up an experimental apparatus for merging beams to study the cluster-cluster collisions in a low energy region. In this article, we report characteristic results obtained in the collision between a neutral argon cluster and a size-selected cobalt dimer ion. This is a typical example of the collision between a cluster of soft matter and a cluster of hard matter. In a low-energy collision, a metal cluster ion can be incorporated into an argon cluster, and then the incorporated metal

cluster turns out to have below liquid argon temperature after the release of some argon atoms.   This method should be compared with the production of a metal cluster in (or on) a rare-gas cluster by using a pick-up cell [13-17, 22].   For example, a silver cluster has been produced in an argon cluster by the pick-up of silver atoms, and optical properties have been measured at a low temperature [22].   In contrast, without preparing rare-gas clusters in advance, a cryogenic drift tube or ion trap is also utilized to attach helium atoms onto an ionic species [23-25].   More generally, argon-attached metal clusters have been produced in argon-mixed carrier gas [26, 27], and their optical absorption spectra have been measured.   Our method presented here suggests a possibility to attach argon atoms onto a size-selected metal cluster ion.   In the future, we can also perform the spectroscopic measurements of the cold cluster ions in a higher resolution by using this merging-beam type collision apparatus.

2. Experimental

A schematic drawing of the apparatus employed is shown in Figure 1.   Cobalt cluster ions were produced in Source 1 by using laser ablation.   A rotating and reciprocating cobalt disk (99.9% in purity) was ablated by pulsed green light (wavelength of 532 nm, repetition rate of 10 Hz, pulse width of ~5 ns, energy of < 10 mJ/pulse) focused on the disk surface from an Nd:YAG laser (Tempest 50, New Wave Research).   Source 1 was mounted on a cold head cooled by liquid nitrogen, and generated cobalt atoms and ions were cooled at the condensation cell in Source 1 by pulsed helium gas (stagnation pressure of 1.5 bar, pulse duration of 2.3 ms, repetition rate of 10 Hz) from a solenoid valve (General Valve series 99, Parker Hannifin) with the orifice of 0.5 mm in diameter, and were allowed to aggregate together.   Produced cobalt cluster ions were guided by an octopole ion beam guide (OPIG 1) passing through a deceleration cell with the length of 200 mm, and their translational-energy spread was compressed by the collision with helium gas (~10^{-2} Torr) in the deceleration cell, as reported by Wöste and co-workers in Ref. 28.   Then the cluster ions were mass-selected by a quadrupole mass selector (QMS 1) (GP-203D and 150-QC, Extrel), and allowed to enter another octopole ion beam guide (OPIG 2) by a quadrupole deflector (QDEF).   OPIG 2 consists of eight molybdenum rods with the diameter of 3 mm and the length of 421 mm which are arranged on a 12-mm diameter circle.

Argon clusters were also introduced to OPIG 2, and the mass-selected cobalt cluster ions collided with these argon clusters in OPIG 2 at low collision energies. These argon clusters were prepared by the supersonic expansion of pulsed argon gas

(stagnation pressure of 20 bar, pulse duration of 250 μs, repetition rate of 10 Hz) from a solenoid valve (General Valve series 99, Parker Hannifin) with the orifice of 0.25 mm in diameter (shown as Source 2). The produced argon clusters were separated by a molecular beam skimmer (orifice diameter of 2 mm, Beam Dynamics) placed at 44 mm downstream from the outlet of the valve, passed straight through QDEF, and entered OPIG 2. The cobalt cluster ions caught up and collided with the argon clusters in OPIG 2 (collision region) as shown in the inset of Figure 1.   The typical spread of the translational energy of the cobalt cluster ions was ~1.3 eV (FWHM) in OPIG 2, which was measured by the retarding potential method.   The translational energy of the cobalt cluster ions in OPIG 2 was controlled by adjusting the DC bias of OPIG 2, and typically the mean relative velocity of cobalt cluster ions to argon clusters was regulated in the range of $20 - 4 \times 10^3$ m/s.   The RF voltage applied to OPIG 2 was fixed to 250 V_{p-p}, and its frequency was ~4 MHz.   The cluster ions were trapped in the effective potential generated by the RF electric field.   We confirmed that the trapping efficiency of the product ions was not reduced even at 100 V_{p-p}.   The power supplies for the OPIGs were assembled by reference to Ref. 29.   The product ions, "cluster complexes", were mass-analyzed by another quadrupole mass selector (QMS 2) (GP-203D and 150-QC, Extrel), and detected by a secondary electron multiplier (SEM) (Channeltron 4139S, Photonis).   The electrical signals were processed by a pulse amplifier/discriminator (F-100T, Advanced Research Instruments), and counted by a personal computer.

By using liquid nitrogen coolant at the cold head of Source 1, the intensity of Co_2^+ increased twenty-fold in comparison with that at room temperature while the intensity of Co^+ dropped down to 10%, and they were comparable in the intensity with each other at liquid nitrogen temperature.   Moreover, the shot-by-shot fluctuations of the intensities of the cobalt cluster ions were reduced, and the larger clusters were also obtained.   Here we define the time when the Nd:YAG laser was fired to the cobalt disk target as $t = 0$.   Under a typical condition, a bunch of cobalt dimer ions arrives at the halfway point of OPIG 2 at $t = 1.32$ ms.   The solenoid valve for the argon-cluster production opens at $t = 0.59$ ms, and a bunch of argon clusters overlaps with that of cobalt dimer ions at the halfway point of OPIG 2 at $t = 1.32$ ms.   We cannot measure the actual size distribution of the neutral argon clusters produced, but to confirm the production of clusters at least, we measured mass spectra of the argon cluster ions by using an ionization source just in front of the skimmer.   Figure 2 shows a typical mass spectrum of the argon clusters ionized by the electron impact, which was measured by the SEM arranged at an off-axis position from the argon cluster beam to avoid the non-ionized neutral atoms and clusters which may generate background signals

4

independent of the mass analysis.   The measured mass spectrum has clear peaks of Ar_p^+ ($p \leq 50$), and indicates that larger neutral argon clusters should be originally produced at Source 2 in consideration of the evaporation of the argon atoms from the cluster in the ionization process.   The intensity drop at $p = 20$ in the mass spectrum, which has been already reported [30-35], is also recognized.   When the SEM was set to an on-axis position of the argon cluster beam, we could also detect neutral argon atoms excited by the electron impact.   The observed time profile had a gaussian shape, and the averaged velocity of neutral argon atoms and clusters was estimated to be ~520 m/s from the arrival time of the excited neutrals at the detector.   Buck and co-workers have measured the velocity of argon clusters as 435.8–556.5 m/s at the nozzle temperature of 300 K and the stagnation pressure of 1.5–2.5 bar with their conical nozzles [36].

3. Results and Discussion

Figure 3(a) shows a mass spectrum of the cluster complexes produced by the collision between the neutral argon clusters and the mass-selected Co_2^+ with the relative velocity of 570 m/s.   This relative velocity can be controlled by changing the velocity of Co_2^+, which is ruled through the DC bias of OPIG 2.   This mass spectrum demonstrates that $Co_2^+Ar_n$ is produced up to $n = 30$ at least.   For comparison, a mass spectrum of Co^+Ar_n produced by the collision between neutral argon clusters and Co^+ is also shown in Figure 3(b).   In the mass spectrum of Co^+Ar_n, Co^+Ar_7 has irregularly a large drop in the abundance in comparison with Co^+Ar_6, and the ion intensity decreases smoothly again in $n \geq 7$.   This result indicates that Co^+Ar_6 has a significantly stable structure. The stability of Co^+Ar_6 and the other transition metal ions, M^+Ar_6 (M = Ti, Ni, Nb, Rh and Pt) has been already reported in Refs. 37–41, and it has been suggested that the six argon atoms occupy vertexes of an octahedron where the transition metal ion is located at the center.   In the mass spectrum of $Co_2^+Ar_n$ [see Figure 3(a)], a sudden abundance drop is also found between $n = 6$ and 7, and additionally an abundance rise is recognized at $n = 12$.   This shows that $Co_2^+Ar_6$ and $Co_2^+Ar_{12}$ have relatively stable structures.   Fielicke and co-workers have measured vibrational spectra of Co_n^+Ar ($n = 4–8$), and clearly indicated that the argon atom prefers an on-top site of Co_n^+ [27]. Therefore, it is considered that each cobalt atom in $Co_2^+Ar_6$ holds three argon atoms on the on-top sites and a stable structure of $Ar_3–(Co–Co)^+–Ar_3$ is formed.   Further, in $Co_2^+Ar_{12}$, additional six argon atoms attach onto the bridge site of Co–Co, and make a six-membered ring around the Co–Co bond.   Consequently the twelve argon atoms in

$Co_2^+Ar_{12}$ complete a distorted icosahedral shell around Co_2^+. This might be a possible reason of the higher stability of $Co_2^+Ar_6$ and $Co_2^+Ar_{12}$.

Total intensity of the cluster complexes, $Co_2^+Ar_n$ ($n \geq 1$), is shown as a function of the relative velocity in Figure 4. In the relative velocity (v_{rel}) region of ≤ 200 m/s, the total intensity is inversely proportional to the relative velocity. This suggests that the charge−induced dipole interaction [42, 43] between Co_2^+ and a neutral argon cluster is dominant in the production of the cluster complex, $Co_2^+Ar_n$. The total intensity of $Co_2^+Ar_n$ once levels off in $v_{rel} \geq 200$ m/s, and this shows that a hard-sphere type interaction [43] dominates the collision and the complex production. In the higher relative velocity region ($v_{rel} \geq 1000$ m/s), the complex intensity decreases again. Probably this is because a cobalt dimer ion which collides with an argon cluster at a sufficiently small impact parameter can stop at the inside of the argon cluster. At a grazing collision, where a cobalt dimer ion collides the outer part of an argon cluster, the cobalt dimer ion can break through the argon cluster.

The size distribution of $Co_2^+Ar_n$ depends on the relative velocity of the collision significantly. As shown in Figure 5, the abundance of $Co_2^+Ar_n$ decreases more gently with the increase of n at $v_{rel} = 570$ m/s than at $v_{rel} = 1300$ m/s, and almost levels off at $n \cong 25$. It is assumed that $Co_2^+Ar_n$ is produced via the sequential evaporation of argon atoms from the collisional intermediate, $Co_2^+Ar_N$, as follows,

$$Co_2^+ + Ar_N \rightarrow Co_2^+Ar_N \rightarrow Co_2^+Ar_{N-1} + Ar \rightarrow \ldots \rightarrow Co_2^+Ar_n + (N - n)Ar. \quad (1)$$
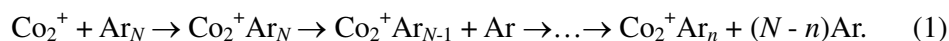
where N and n represent the size of the neutral argon cluster just before the collision and the number of remaining argon atoms after the evaporation respectively. Under employed experimental conditions, the relative velocity of Co_2^+ to Ar_N is constant, and then the collision energy depends on the mass of Ar_N. For example, at $v_{rel} = 570$ m/s, the collision energy is 0.09 eV for Co_2^+ with Ar_2, and 0.21 eV with Ar_{50}. This collision energy and the potential energy difference between $Co_2^+Ar_N$ and $Co_2^+ + Ar_N$ are exhausted in the evaporation of the argon atoms from the collisional intermediate, $Co_2^+Ar_N$. The potential energy difference can be estimated to be the summation of the difference between the bond dissociation energy of $Co_2^+Ar_{N-1}−Ar$ and that of $Ar_{N-1}−Ar$. The bond dissociation energy of $Co_2^+Ar_{N-1}−Ar$ is approximated to be 67 meV from those of argon cluster ions [44], while that of $Ar_{N-1}−Ar$ is considered to be 56 meV [45]. Then the potential energy difference between $Co_2^+Ar_N$ and $Co_2^+ + Ar_N$ turns out to be 0.55 eV at $N = 50$. As a result, the available energy of the collisional intermediate, $Co_2^+Ar_N$, is assumed to be 0.76 eV (= 0.55 eV + 0.21 eV) totally, and it is considered

6

that eleven argon atoms can evaporate from $Co_2^+Ar_N$ at $N = 50$ energetically. This energetics is combined with a log-normal distribution of Ar_N [46], and a size distribution of $Co_2^+Ar_n$ is estimated.

The beam diameter of Co_2^+ at the collision region is supposed to be smaller than that of Ar_N because the divergence of Co_2^+ is limited by the effective potential of OPIG 2 while the beam of Ar_N is independent of the electric field. This means that all of Co_2^+ have the possibility to be incorporated into Ar_N. The intensity of the collisional intermediate, $I_{Co_2^+Ar_N}(v_{rel}, N)$, is estimated as follows,

$$I_{Co_2^+Ar_N}(v_{rel}, N) = I_{Co_2^+}(v_{rel}) \times I_{Ar_N}(N) \times P_{inc}(v_{rel}, N) \quad (2)$$

where $I_{Co_2^+}(v_{rel})$, $I_{Ar_N}(N)$, and $P_{inc}(v_{rel}, N)$ represent the intensity of Co_2^+ with a certain relative velocity, the intensity of Ar_N with a log-normal distribution, and the incorporation probability between the clusters respectively. The distribution of the relative velocity of Co_2^+, $I_{Co_2^+}(v_{rel})$, was experimentally measured, and the total intensity of Co_2^+ was set to unity. In equation (2), the incorporation probability P_{inc} is estimated as follows,

$$P_{inc}(v_{rel}, N) = \sigma(v_{rel}, N) d_{Ar_N} l_{Ar_N} P_{Co_2^+Ar_N}(v_{rel}) \quad (3)$$

where $\sigma(v_{rel}, N)$, d_{Ar_N}, l_{Ar_N}, and $P_{Co_2^+Ar_N}(v_{rel})$ represent the collision cross section, the number density of Ar_N in a bunch, the spatial length of the Ar_N bunch, and the probability of $Co_2^+Ar_N$ production respectively. $P_{Co_2^+Ar_N}(570 m/s)$ and $P_{Co_2^+Ar_N}(1300 m/s)$ were relatively evaluated from the total intensity of $Co_2^+Ar_n$ (shown in Figure 4). In fact, the product $d_{Ar_N} l_{Ar_N} P_{Co_2^+Ar_N}$ is adjusted to reproduce the relative intensity of $Co_2^+Ar_n$. Since the hard-sphere interaction is assumed to dominate the

collision between Co_2^+ and Ar_N in $v_{rel} \geq 200$ m/s, $\sigma(v_{rel}, N)$ is represented by the hard-sphere cross section as follows,

$$\sigma(v_{rel}, N) = \pi \left(r_{Ar_N} + r_{Co_2^+} \right)^2 \quad (4)$$

where r_{Ar_N} and $r_{Co_2^+}$ represent the radii of Ar_N and Co_2^+ respectively. The shapes of the clusters are supposed to be spherical, and these radii are obtained from the densities of solid argon [47] and cobalt [48].

The collisional intermediate, $Co_2^+Ar_N$, has the internal energy corresponding to the summation of the collision energy and the potential energy difference as described above. The internal energy of $Co_2^+Ar_N$ is relaxed via the sequential evaporation of argon atoms, and finally $Co_2^+Ar_N$ becomes $Co_2^+Ar_n$. The relation between N and n, $k(v_{rel}, N, n)$, is estimated from the energetics. The simulated intensity of cluster complexes, $I_{Co_2^+Ar_n}(n)$, is given by the product of (2) with $k(v_{rel}, N, n)$ as follows,

$$I_{Co_2^+Ar_n}(n) = \sum_N k(v_{rel}, N, n) I_{Co_2^+Ar_N}(v_{rel}, N). \quad (5)$$

The simulated size distributions of $Co_2^+Ar_n$ reproduce those experimentally obtained quite well as shown in Figure 5. This indicates that these assumptions are appropriate for the explanation of the production mechanism of $Co_2^+Ar_n$, and the log-normal distribution and the sequential evaporation play essential roles in this model.

In summary, the cluster complex between a size-selected cobalt dimer ion and a neutral argon cluster was successfully produced by using a merging-beam technique in a pulsed mode. The detected largest cluster complex was $Co_2^+Ar_{30}$, and these cluster complexes were produced through the evaporation of argon atoms from the collisional intermediate, $Co_2^+Ar_N$. The intensity of the produced cluster complexes increases steeply with the decrease of the relative velocity between the clusters in $v_{rel} \leq 200$ m/s. The intensity levels off in the region of 200 m/s $\leq v_{rel} \leq 1000$ m/s and decreases in $v_{rel} \geq 1000$ m/s. This shows that the collision between the clusters occurs mainly based on the charge–induced dipole interaction and hard-sphere interaction below and above the

relative velocity of 200 m/s respectively. In the relative velocity higher than 1000 m/s, the hard-sphere interaction is dominant but the incorporation probability becomes lower.

Acknowledgments

References

(1) R. Ferrando, J. Jellinek and R. L. Johnston, *Chem. Rev.*, 2008, **108**, 845-910.

(2) J. Graciani, K. Mudiyanselage, F. Xu, A. E. Baber, J. Evans, S. D. Senanayake, D. J. Stacchiola, P. Liu, J. Hrbek, J. F. Sanz and J. A. Rodriguez, *Science*, 2014, **345**, 546-550.

(3) A. C. Cardiel, M. C. Benson, L. M. Bishop, K. M. Louis, J. C. Yeager, Y. Tan and R. J. Hamers, *ACS Nano*, 2012, **6**, 310-318.

(4) D. K. Kim, D. Kan, T. Veres, F. Normadin, J. K. Liao, H. H. Kim, S.-H. Lee, M. Zahn and M. Muhammed, *J. Appl. Phys.*, 2005, **97**, 10Q918.

(5) S. Nonose, Y. Sone, K. Onodera, S. Sudo and K. Kaya, *J. Phys. Chem.*, 1990, **94**, 2744-2746.

(6) E. Janssens, T. V. Hoof, N. Veldeman, S. Neukemans, M. Hou and P. Lievens, *Int. J. Mass Spectrom.*, 2006, **252**, 38-46.

(7) K. Miyajima, N. Fukushima and F. Mafuné, *J. Phys. Chem. A*, 2009, **113**, 4858-4861.

(8) S. H. Xie, H. Tsunoyama, W. Kurashige, Y. Negishi and T. Tsukuda, *ACS Catal.*, 2012, **2**, 1519-1523.

(9) X. Yuan, X. Dou, K. Zheng and J. Xie, *Part. Part. Syst. Charact.*, 2015, **32**, 613-629.

(10) S. Wang, Y. Song, S. Jin, X. Liu, J. Zhang, Y. Pei, X. Meng, M. Chen, P. Li and M Zhu, *J. Am. Chem. Soc.*, 2015, **137**, 4018-4021.

(11) M. Di Vece, N. P. Young, Z. Li, Y. Chen and R. E. Palmer, *Small*, 2006, **2**, 1270-1272.

(12) R. Alayan, L. Arnaud, M. Broyer, E. Cottancin, J. Lermé, S. Marhaba, J. L. Vialle and M. Pellarin, *Phys. Rev. B*, 2007, **76**, 075424.

(13) J. P. Toennies and A. F. Vilesov, *Angew. Chem. Int. Ed.*, 2004, **43**, 2622-2648

(14) S. Yang and A. M. Ellis, *Chem. Soc. Rev.*, 2013, **42**, 472-484.

(15) A. Boatwright, C. Feng, D. Spence, E. Latimer, C. Binns, A. M. Ellis and S. Yang, *Faraday Discuss.*, 2013, **162**, 113-124.

(16) P. Thaler, A. Volk, F. Lackner, J. Steurer, D. Knez, W. Grogger, F. Hofer and W. E. Ernst, *Phys. Rev. B*, 2014, **90**, 155442.

(17) S. B. Emery, Y. Xin, C. J. Ridge, R. J. Buszek, J. A. Boatz, J. M. Boyle, B. K. Little and C. M. Lindsay, *J. Chem. Phys.*, 2015, **142**, 084307.

(18) V. Singh, C. Cassidy, P. Grammatikopoulos, F. Djurabekova, K. Nordlund, M. Sowwan, *J. Phys. Chem. C*, 2014, **118**, 13869-13875.

(19) R. Schmidt, G. Seifert and H. O. Lutz, *Phys. Lett. A*, 1991, **158**, 231-236.

(20) R. Schmidt, G. Seifert and H. O. Lutz, in "Nuclear Physics Concepts in the Study of Atomic Cluster Physics", Lecture Notes in Physics; Springer: Berlin, Germany, 1992, **404**, 128-141.

(21) F. Rohmund, E. E. B. Campbell, O. Knospe, G. Seifert and R. Schmidt, *Phys. Rev. Lett.*, 1996, **76**, 3289-3292.

(22) W. Christen, P. Radcliffe, A. Przystawik, Th. Diederich and J. Tiggesbäumker, *J. Phys. Chem. A*, 2011, **115**, 8779-8782.

(23) H. Tanuma, J. Sanderson and N. Kobayashi, *J. Phys. Soc. Jpn.*, 1999, **68**, 2570-2575.

(24) F. Grandinetti, *Int. J. Mass Spectrom.*, 2004, **237**, 243-267.

(25) K. R. Asmis, *Phys. Chem. Chem. Phys.*, 2012, **14**, 9270-9281.

(26) (a) W. J. C. Menezes and M. B. Knickelbein, *J. Chem. Phys.*, 1993, **98**, 1856-1866; (b) M. B. Knickelbein, *J. Chem. Phys.*, 1993, **99**, 2377-2382.

(27) R. Gehrke, P. Gruene, A. Fielicke, G. Meijer and K. Reuter, *J. Chem. Phys.*, 2009, **130**, 034306.

(28) (a) S. Wolf, G. Sommerer, S. Rutz, E. Schreiber, T. Leisner, L. Wöste and R. S. Berry, *Phys. Rev. Lett.*, 1995, **74**, 4177-4180; (b) T. Leisner, S. Vajda, S. Wolf, L. Wöste and R. S. Berry, *J. Chem. Phys.*, 1999, **111**, 1017-1021.

(29) I. Cermak, *Rev. Sci. Instrum.*, 2005, **76**, 063302.

(30) T. A, Milne and F. T. Greene, *J. Chem. Phys.*, 1967, **47**, 4095-4101

(31) R. G. Orth, H. T. Jonkman, D. H. Powell and J. Michl, *J. Am. Chem. Soc.*, 1981, **103**, 6026-6030

(32) A. Ding and J. Hesslich, *Chem. Phys. Lett.*, 1983, **94**, 54-57

(33) D. R. Worsnop, S. J. Buelow and D. R. Herschbach, *J. Phys. Chem.*, 1984, **88**, 4506-4509

(34) T. D. Märk, P. Scheier, K. Leiter, W. Ritter, K. Stephan and A. Stamatovic, *Int. J. Mass Spectrom. Ion Processes*, 1986, **74**, 281-301

(35) M. Ichihashi, S. Nonose, T. Nagata and T. Kondow, *J. Chem. Phys.*, 1994, **100**, 6458-6463.

(36) U. Buck, R. Krohne and P. Lohbrandt, *J. Chem. Phys.*, 1997, **106**, 3205-3215.

(37) D. Lessen and P. J. Brucat, *Chem. Phys. Lett.*, 1988, **149**, 10-13.

(38) M. Beyer, C. Berg, G. Albert, U. Achatz and V. E. Bondybey, *Chem. Phys. Lett.*, 1997, **280**, 459-463.

(39) M. Velegrakis, G. E. Froudakis and S. C. Farantos, *J. Chem. Phys.*, 1998, **109**,

4687-4688.

(40) M. Velegrakis, G. E. Froudakis and S. C. Farantos, *Chem. Phys. Lett.*, 1999, **302**, 596-601.

(41) G. E. Froudakis, M. Muhlhauser, S. C. Farantos, A. Sfounis and M. Velegrakis, *Chem. Phys.*, 2002, **280**, 43-51.

(42) G. Gioumousis and D. P. Stevenson, *J. Chem. Phys.*, 1958, **29**, 294-299.

(43) R. D. Levine, *Molecular Reaction Dynamics* (Cambridge University Press, Cambridge, United Kingdom, 2005)

(44) K. Hiraoka and T. Mori, *J. Chem. Phys.*, 1989, **90**, 7143-7149.

(45) J. Farges, M. F. de Feraudy, B. Raoult and G. Torchet, *J. Chem. Phys.*, 1986, **84**, 3491-3501.

(46) M. Lewerenz, B. Schilling and J. P. Toennies, *Chem. Phys. Lett.*, 1993, **206**, 381-387.

(47) O. G. Peterson, D. N. Batchelder and R. O. Simmons, *Phys. Rev.*, 1966, **150**, 703.

(48) D. R. Lide and H. P. R. Frederikse (editors), *CRC Handbook of Chemistry and Physics 78th ed.*, CRC Press, New York, USA, 1997.

Figure Captions

Figure 1

Schematic drawing of the experimental setup. (Source 1) a cobalt cluster ion source composed of a pulsed valve and a condensation cell with laser ablation, (OPIG 1) an octopole ion beam guide which passes through a deceleration cell filled with He gas, (QMS 1) a quadrupole mass selector for size selection of cobalt cluster ions, (QDEF) a quadrupole deflector for cobalt cluster ions, (Source 2) a pulsed valve for production of argon clusters, (OPIG 2) an octopole ion beam guide for merging the cobalt cluster ion beam with the argon cluster beam, (QMS 2) a quadrupole mass selector for mass analysis of produced cluster complexes, (SEM) a secondary electron multiplier for ion counting measurements. Spatial and temporal overlap of the bunch of Co_2^+ with that of Ar_N is schematically shown in the inset.

Figure 2

Mass spectrum of Ar_p^+ obtained from Ar_N with the electron impact ionization. Acceleration voltage of the electrons and the emission current were 70 V and ~100 μA, respectively.

Figure 3

(a) Mass spectrum of $Co_2^+Ar_n$ produced by the collision between Co_2^+ and Ar_N. (b) Mass spectrum of Co^+Ar_n produced by the collision between Co^+ and Ar_N. Intensities of both product ions were normalized with unreacted Co_2^+ and Co^+, respectively.

Figure 4

Total intensity of the collision products, $Co_2^+Ar_n$ ($n = 1-30$), plotted as a function of the relative velocity. The total intensities are indicated as the relative values to the intensity of Co_2^+. The solid line is proportional to $1/v_{rel}$.

Figure 5

Size distributions of $Co_2^+Ar_n$ produced by the collision between Co_2^+ and Ar_N. Red circles and open squares represent the relative intensities of $Co_2^+Ar_n$ at the relative velocities of 570 and 1300 m/s respectively. The red and the black curves show the relative intensities obtained from the simulations (see text) at the relative velocities of 570 and 1300 m/s respectively.
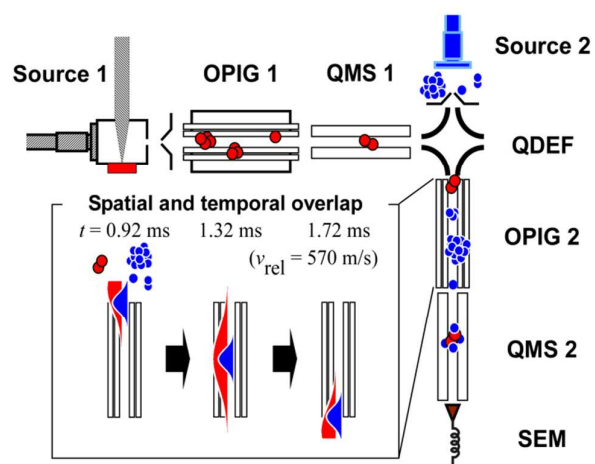
Figure 1. H. Odaka *et al.*
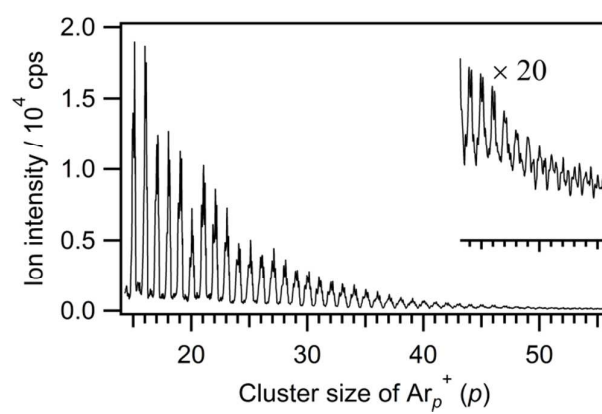
Figure 2. H. Odaka *et al.*
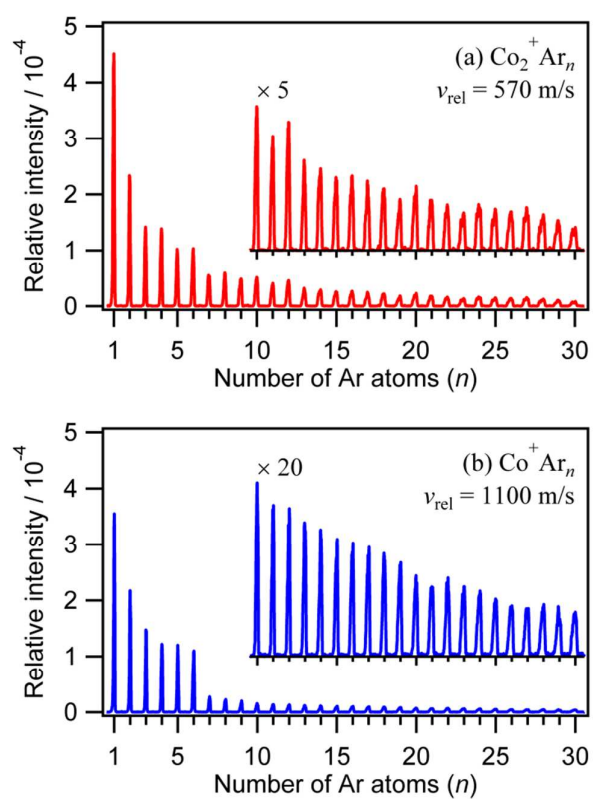
Figure 3. H. Odaka *et al.*
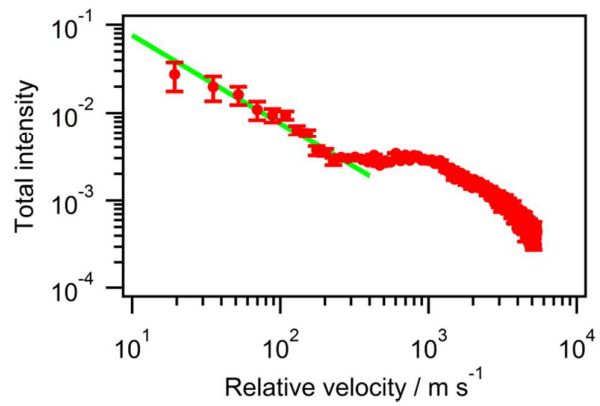
Figure 4. H. Odaka *et al.*
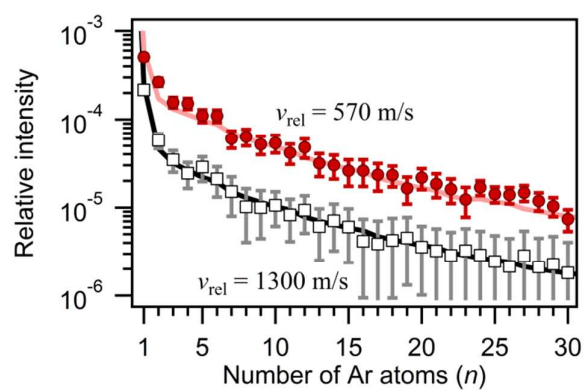
Figure 5. H. Odaka *et al.*

TOC entry

Size-selected cobalt dimer cations are incorporated into neutral argon clusters by using a merging-beam technique in a pulsed mode. The incorporation process is explained on the basis of the electrostatic interaction and the hard-sphere interaction below and above the relative velocity of 200 m/s respectively.